ORIGINAL ARTICLE

Dual-polarized ratio algorithm for retrieving Arctic sea ice concentration from passive microwave brightness temperature

Shugang Zhang · Jinping Zhao · Karen Frey · Jie Su

Abstract We present a new algorithm for retrieving sea ice concentration from the AMSR-E data, the dual-polarized ratio (DPR) algorithm. The DPR algorithm is developed using vertically and horizontally polarized brightness temperatures at the same channel of 36.5 GHz. It depends on the ratio of dual-polarized emissivity, α, which is determined empirically at about 0.92 by remotely sensed brightness temperature in winter and used for the other seasons as well. The ice concentration retrieved by the DPR is compared with those by the NT2 and ABA algorithms. Since the main difference among these algorithms takes place in marginal ice zones, 17 marginal ice zones are chosen. The retrieved ice concentrations in these zones are examined by the ice concentration obtained by the MODIS data. The mean error, root-mean-square error and mean absolute error of the DPR algorithm are relatively better than those from the other two algorithms. The results of this study illustrate that the DPR algorithm is a more accurate algorithm for retrieving sea ice concentration from the AMSR-E brightness temperature, and can be used for operational purposes.

Keywords Arctic · Ice concentration · AMSR-E · Brightness temperature · Dual-polarized ratio algorithm

S. Zhang (✉) · J. Zhao · J. Su
Ocean University of China, Qingdao,
People's Republic of China
e-mail: zhangshugang6@163.com

J. Zhao
e-mail: jpzhao@ouc.edu.cn

K. Frey
Clark University, Worcester, USA

1 Introduction

Polar regions play an important role in the global climate system and the energy balance. Furthermore, Arctic sea ice is a key environmental variable and is a sensitive indicator of global warming (Lemke 1987; Comiso et al. 2003). The sea ice albedo of more than 0.8 for the predominantly snow-covered seasonal ice or multi-year ice is much higher than that of the open ocean of about 0.1 (Grenfell 1983; Comiso et al. 2003), which results in a sharp contrast in surface energy flux between the marginal ice zone and the open ocean. Sea ice is an effective insulator that restricts the exchanges of energy and momentum between the ocean and the atmosphere. During wintertime, the heat flux through open water is two orders of a magnitude higher than that through thick ice (Maykut 1978). Sea ice also alters oceanic structure and circulation during ice growing or melting stages. For example, the cold and dense water formed from sea ice growth in the Arctic leads and polynyas helps to maintain the halocline in the Arctic Ocean (Aagaard et al. 1981; Cavalieri and Martin 1994). So it is important to monitor sea ice extent and its physical property in different seasons and regions to reveal the energy exchange between ocean and atmosphere.

As the most important parameter of sea ice, ice concentration can be used to study variation of sea ice distribution, marginal ice zone, and leads and polynyas (Cavalieri and Martin 1994; Zwally et al. 2002). Satellite passive microwave remote sensing has become a useful tool to monitor sea ice concentration day and night, because microwave signals can penetrate thick cloud and other substances in the atmosphere. Sea ice is easily distinguished from open water because their emissivities are quite different (Zwally et al. 1983). The Advanced Microwave Scanning Radiometer-EOS (AMSR-E) sensor on board the EOS-Aqua

launched on May 4, 2002 measures vertically and horizontally polarized radiances at 6.925, 10.65, 18.7, 23.8, 36.5, and 89.0 GHz. The microwave radiance for each frequency can be expressed as a brightness temperature according to the Rayleigh–Jeans Law (Liou 2002).

Several algorithms of retrieving sea ice concentration from brightness temperature data have been developed (Cavalieri et al. 1984; Comiso 1986; Svendsen et al. 1987; Smith 1996; Comiso et al. 1997; Markus and Cavalieri 2000). A brief description of these algorithms and comparison of some ice concentration results was presented by Andersen et al. (2007). There are three main algorithms for retrieving sea ice concentration from the AMSR-E brightness temperature data: (1) the AMSR Bootstrap Algorithm (ABA; Comiso et al. 2003); (2) the NT2 algorithm from the enhanced NASA Team (Markus and Cavalieri 2000); (3) the ARTIST Sea Ice (ASI) algorithm (Spreen et al. 2008). The ABA is slightly modified from the Bootstrap Algorithm (BBA; Comiso et al. 2003). The difference between the two is that the BBA uses brightness temperature (Comiso 1995), but the ABA uses sea ice surface emissivity instead. The emissivity of sea ice is calculated by brightness temperature data of 6.9, 18.7, and 36.5 GHz. The National Snow and Ice Data Center (NSIDC) of the US provides the 12.5×12.5 km gridded AMSR-E brightness temperature and sea ice concentration inferred from the ABA and NT2 algorithms at the same grid (http://nsidc.org/data/amsre). The ASI is a special algorithm for retrieving high-resolution sea ice concentration using the brightness temperature data at 89 GHz.

The retrieval accuracy by each algorithm is limited by its physical background when it is applied to the low-resolution microwave data. It is therefore necessary to develop new algorithms with novel physical considerations to improve the accuracy of the derived ice concentration. We developed a simple and effective algorithm for sea ice concentration using dual-polarized brightness temperature at the same channel in this study. The AMSR-E brightness temperature data of 12.5×12.5 km at 36.5 GHz is used, and the retrieved ice concentrations by this and other algorithms are validated using the simultaneous Moderate Resolution Imaging Spectroradiometer (MODIS) data. The advantages of this algorithm are f higher precision, lower bias, and higher stability when compared with other algorithms.

2 Dual-polarized ratio algorithm for retrieving sea ice concentration

The new sea ice concentration algorithm is referred to as the dual-polarized ratio (DPR) algorithm. The DPR algorithm takes advantage of the close correlation between sea ice concentration and dual-polarized microwave radiation.

The ratio of the two polarized emissivities of ice can be obtained from the ratio of brightness temperature of the pixels with 100 % ice concentration. Using this physical relationship, a more accurate algorithm for sea ice concentration is derived.

2.1 Dual-polarized ratio algorithm

Sea ice concentration algorithms, such as the DPR, NT2, and ABA, are all developed from the basic radiative transfer equation that expresses the relation of brightness temperatures at different frequencies. Comiso and Zwally (1982) pointed out that brightness temperature in regions covered by sea ice is contributed by ice, water, and atmosphere temperatures. As the net effect of atmosphere temperature is very small and therefore negligible (Wilheit 1980; Comiso and Sullivan 1986; Comiso et al. 1994), the brightness temperature T_b could be considered as a function of sea ice temperature T_i and water temperature T_w,

$$T_b = \varepsilon_i T_i C + \varepsilon_w T_w (1 - C), \tag{1}$$

where C is ice concentration, ε_i and ε_w are ice microwave emissivity and sea water microwave emissivity, respectively. In Eq. (1), T_b is acquired from satellite observations, but C, T_i, and T_w are unknown. Let the vertically and horizontally polarized brightness temperatures be T_{b1} and T_{b2}, the vertically polarized sea ice and water emissivities be ε_{i1} and ε_{w1}, the horizontally polarized sea ice and water emissivities be ε_{i2} and ε_{w2}, T_{b1} and T_{b2} can be written as

$$T_{b1} = \varepsilon_{i1} T_i C + \varepsilon_{w1} T_w (1 - C), \tag{2a}$$

$$T_{b2} = \varepsilon_{i2} T_i C + \varepsilon_{w2} T_w (1 - C). \tag{2b}$$

Sea ice concentration can be derived from Eq. (2):

$$C = 1 + \frac{\varepsilon_{i2} T_{b1} - \varepsilon_{i1} T_{b2}}{T_w (\varepsilon_{w2} \varepsilon_{i1} - \varepsilon_{w1} \varepsilon_{i2})}. \tag{3}$$

Comiso et al. (1984) derived a similar equation as Eq. (3) with little difference. They suggested that sea ice concentration cannot be calculated by Eq. (3) directly unless sea ice and water emissivities are known exactly. Unfortunately, ε_{i1} and ε_{i2} vary seasonally and regionally, and cannot be determined exactly. Thereby, the ice concentration by Eq. (3) may bring unacceptable error. As a result, Eq. (3) has never been used to retrieve sea ice concentration.

In this paper, the new algorithm of DPR is proposed to avoid the influence of uncertain sea ice emissivity in order to obtain more accurate sea ice concentration. Equation (3) can be written as

$$C = 1 + \frac{\alpha T_{b1} - T_{b2}}{T_w (\varepsilon_{w2} - \varepsilon_{w1} \alpha)}, \tag{4}$$

where

$$\alpha = \frac{\varepsilon_{i2}}{\varepsilon_{i1}}. \tag{5}$$

As the emissivities of seawater changes a little, if the value of α is known, the sea ice concentration can be calculated according to Eq. (4). Figure 1 is the scatter plot of the vertically and horizontally polarized AMSR-E brightness temperatures at 36.5 GHz for the Arctic. The dots corresponding to 100 % ice concentration distribute along the line AD in Fig. 1 (Comiso 1995; Comiso et al. 2003). So for a 100 % ice concentration, Eq. (2) can be written as

$$T_b(V36.5) = \varepsilon_i(V36.5)T_i,$$
$$T_b(H36.5) = \varepsilon_i(H36.5)T_i.$$

By combining the two equations and Eq. (5),

$$T_b(H36.5) = \frac{\varepsilon_i(H36.5)}{\varepsilon_i(V36.5)} \cdot T_b(V36.5) = \alpha \cdot T_b(V36.5). \tag{6}$$

Equation (6) indicates that the Line AD in Fig. 1 passes through the point (0,0) and α in Eq. (4) is the slope of the line in the brightness temperature space. The clustering of the dots in Fig. 1 also tells us that although ε_{i1} and ε_{i2} are not exactly known, their ratio α is nearly a constant. The approximate
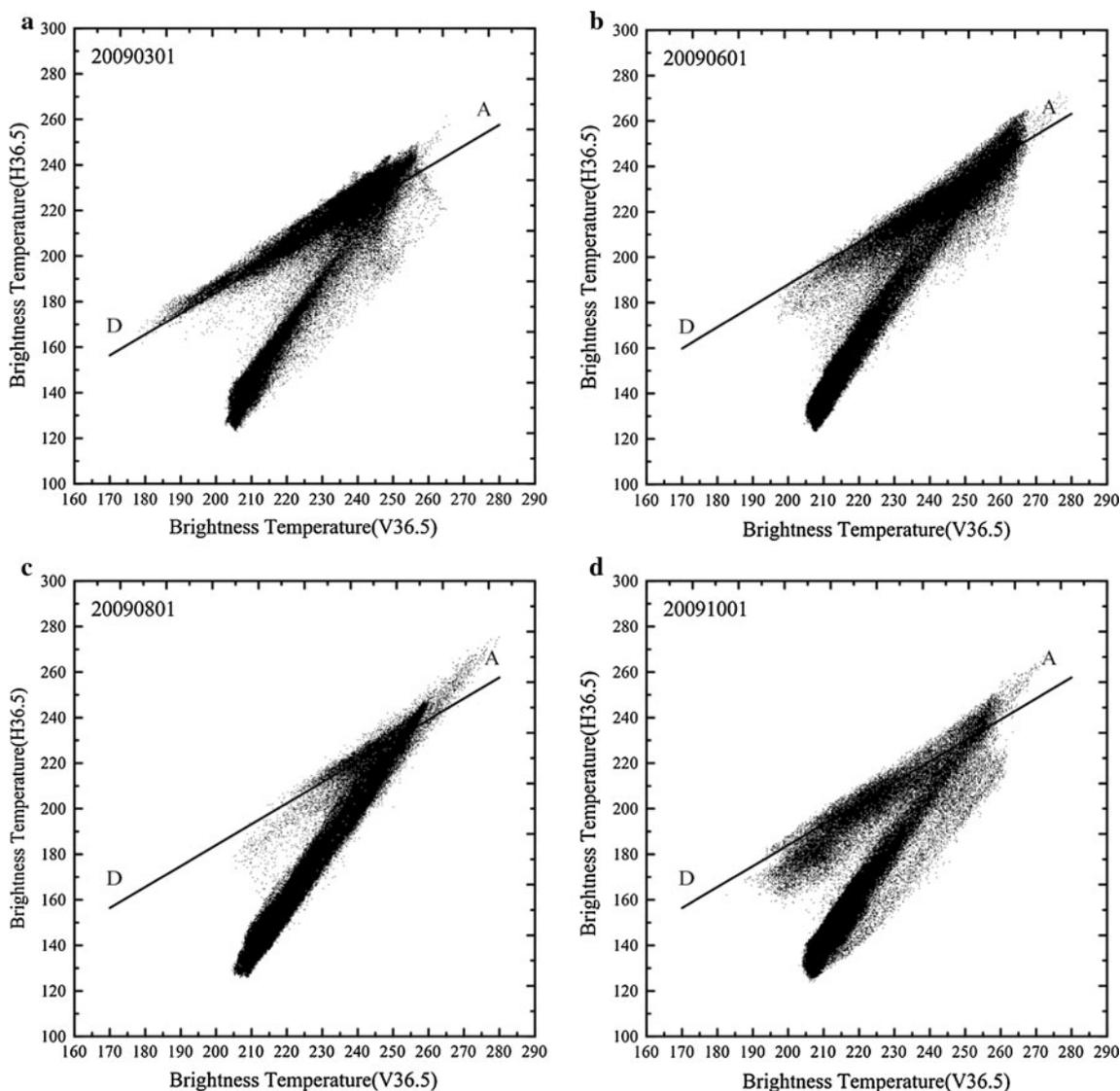
Fig. 1 Scatter plot of the dual-polarized brightness temperature at 36.5 GHz at 2009: March 1 (**a**), June 1 (**b**), August 1 (**c**), and October 1 (**d**). The slope of line AD is 0.92

constant property of α indicates that the vertically and horizontally polarized brightness temperatures are highly associated no matter how different the surface properties of sea ice and snow are. This association could be considered as one of the physical properties of microwave radiation from sea ice surface.

In Eq. (4), ε_{w1}, ε_{w2}, and T_w need to be pre-assigned for retrieving sea ice concentration. The open water inside the ice pack normally has a smooth surface because the wave effect has been attenuated by ice floes (Comiso 1995). So ε_{w1} and ε_{w2} can be determined by the emissivity of calm sea water (Svendsen et al. 1983). Sea water temperature T_w inside the ice pack or marginal ice zone could be chosen as the freezing point approximately. With these known parameters, the dual-polarized brightness temperature at 36.5 GHz can be used to retrieve sea ice concentration according to Eq. (4).

2.2 Determination of α

The analysis above suggests that sea ice concentration can be retrieved when α is determined. It will be significant to develop a method to determine α, because the ice concentration is quite sensitive to the α.

Actually, α is also the ratio of horizontally and vertically polarized brightness temperatures according to Eq. (6). The ratio γ of all the dual-polarized brightness temperatures in winter is defined as

$$\gamma = \frac{T_b(H36.5)}{T_b(V36.5)}, \tag{7}$$

and α will be a value of a certain γ. The spatial distribution of γ is shown in Fig. 2a. It can be seen that γ is approximately a constant in a large Arctic region for the 100 % ice concentration, though the brightness temperature in the Arctic varies over a large range. In Fig. 2b, two zero-crossing lines are shown in a scatter plot. The slope of the blue line is 0.92 and ofthe red line is 0.97. It is apparent that the data points linearly distribute between the blue line and the red line. The results indicate that a minimum γ should be determined first. When γ is larger than the minimum γ, sea ice concentration will be assigned to one. In marginal ice zone, sea ice concentration is less than 1, and the change of γ is obvious (from 0.77 to 0.92).

Fig. 2 The methods for determining α by the dual-polarized brightness temperature at 36.5 GHz on January 1, 2009. **a** Map of γ in Arctic and contour interval is 0.02; **b** scatter plot of the dual-polarized brightness temperature at 36.5 GHz at January 1. The slopes of the *blue* and *red* zero-crossing lines are 0.92 and 0.97, respectively; **c** histogram of γ; and **d** the frequency (γ) gradient frequency of γ. The slope of solid line AD in Fig. 1 correspond to the dot line AD in the **c** and **d**
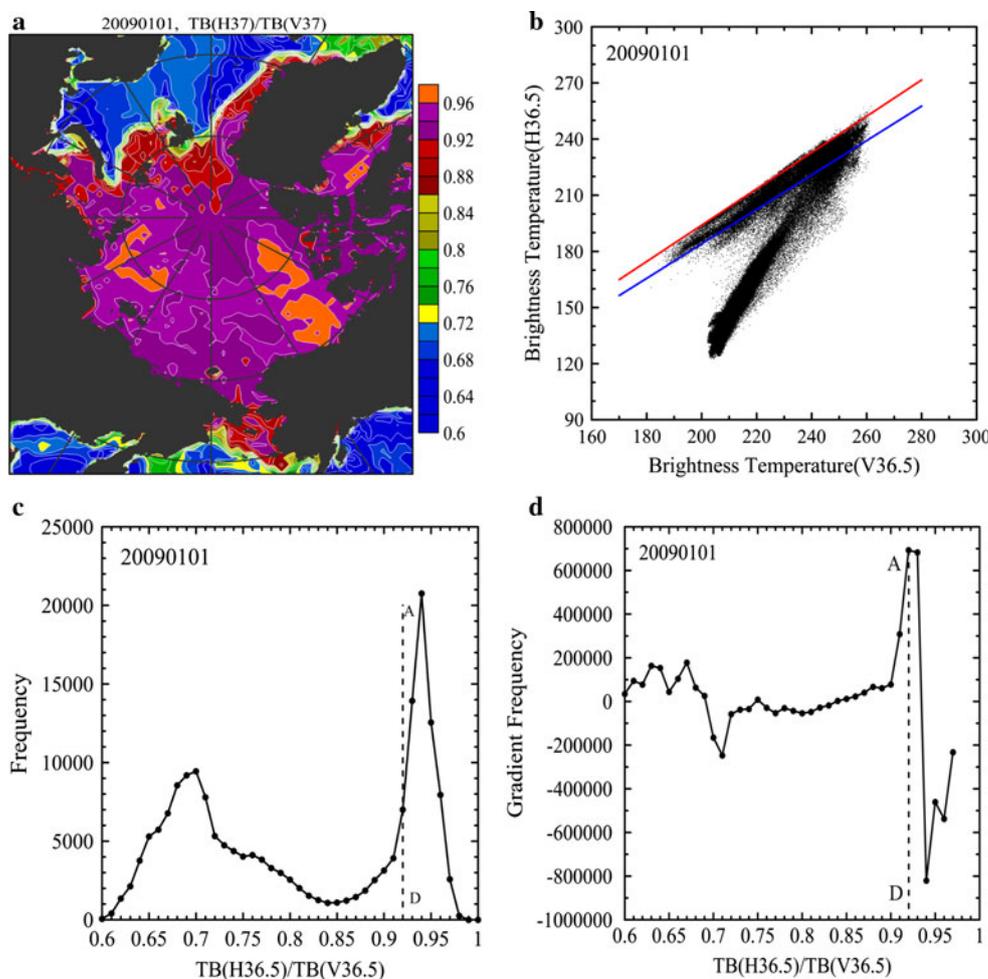
Figure 2c shows the frequency histogram of γ calculated by Eq. (7) for the whole Arctic region. Two peaks appear: the left one corresponds to open water, and the right one corresponds to high sea ice concentration according to Fig. 2a. The parameter γ changes very little in terms of values (Fig. 2a), but changes greatly in terms of frequency (Fig. 2c). Because the amount of sea ice pixels is large and the amount of the MIZ is small, the minimum γ with 100 % ice concentration should equal the value where the frequency of γ changes the steepest. The frequency gradient of γ is calculated and shown in Fig. 2d, indicating the largest frequency gradient is at 0.92. This value is just the minimum γ for 100 % ice concentration, and is defined as α in Eq. (4). Sea ice concentration is taken as 1 when γ is larger than α. Therefore, the α could be determined directly by the ratio of two polarized brightness temperatures as shown in Fig. 2.

Sea ice concentration in winter can be retrieved using Eq. (4), namely, the DPR algorithm. It is difficult to determine α using summertime data by the method, because there are fewer pixels with 100 % sea ice concentration, such as in Fig. 1c. However, the results of Sect. 3 indicates that α determined by winter brightness temperature could be used in summer. So the DPR algorithm using the dual-polarized brightness temperature at 36.5 GHz could be used to retrieve sea ice concentration for all seasons.

Because α is empirically obtained by the extreme of the frequency gradient, it cannot be adjusted easily. As a result, the DPR algorithm is a more objective method for ice concentration retrieval.

2.3 Method to determine the margin of sea ice

After the ice concentration is retrieved using Eq. (4), a criterion is needed to distinguish sea ice and open water when the concentration is close to zero. This criterion is necessary to determine the margin of ice cover. Heinrichs et al. (2006) point out that the position of the ice edge determined from AMSR-E data using a 15 % concentration threshold was found to be, on average, within one AMSR-E grid square (12.5 × 12.5 km), but this criterion is inappropriate to retrieve sea ice concentration using Eq. (4). The main reason is that the dual-polarized brightness temperature at 36.5 GHz could not distinguish the position of the ice edge (Fig. 2a). Several studies suggested that

Fig. 3 The method for determining β by the vertically polarized brightness temperatures at 18.7 and 36.5 GHz on January 1, 2009. **a** Map of γ in Arctic and *black line* is contour for 15 % sea ice concentration; **b** scatter plot of the vertically polarized brightness temperatures at 18.7 and 36.5 GHz at January 1. The slope of the red zero-crossing line is 0.89; **c** histogram of θ; and **d** the frequency(θ) gradient. The slope of solid line OW in Fig. 3b corresponds to the dot line OW in the **c** and **d**
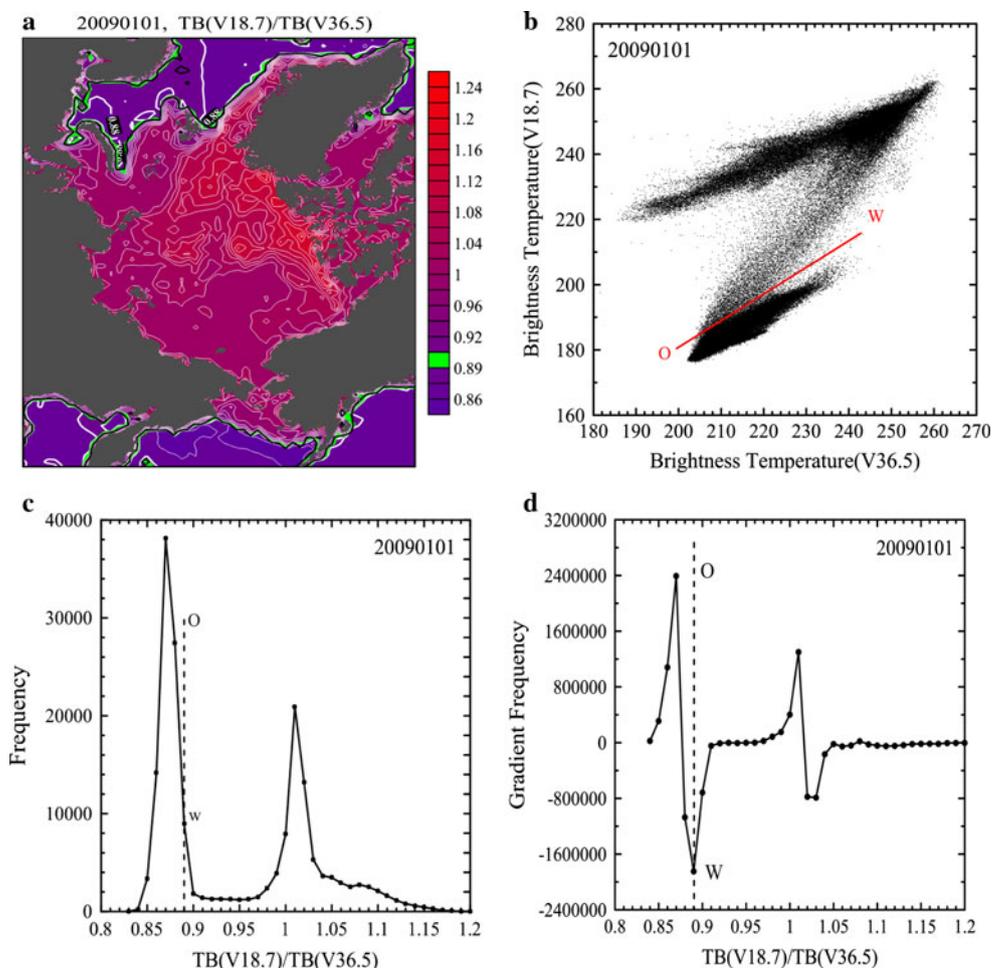
vertically polarized brightness temperature at 18.7 and 36.5 GHz could be used to distinguish the marginal of ice cover (Comiso et al. 1984; Comiso and Sullivan 1986). The brightness temperatures at these two channels are shown in Fig. 3b. The sea ice concentration is zero or approximately zero when the cluster of dots is along the line OW. So, the interface of sea ice and open water can be defined using the AMSR-E brightness temperatures at 18.7 and 36.5 GHz.

Similarly, a parameter θ, which is the ratio of vertically polarized brightness temperatures at 18.7 and 36.5 GHz, is defined as

$$\theta = \frac{T_b(V18.7)}{T_b(V36.5)}. \tag{8}$$

The spatial distribution of θ is shown in Fig. 3a. Isobars 0.89 (green) are marked in the figure, and the margin of ice cover can be distinguished clearly. At same time, the black line in the figure is the contour for 15 % sea ice concentration, which is calculated by Eq. (4).

There are two peaks in the histogram (Fig. 3c) of θ: the left one corresponds to open water, and the other corresponds to sea ice with the concentration of 1. The frequency of θ changes obviously at the marginal ice zone. Similar to determining α, a maximum θ for open water should appear where the frequency of θ changes the most. Figure 3d show the least frequency gradient lies at 0.89, which is defined as β. The physical meaning of β is the
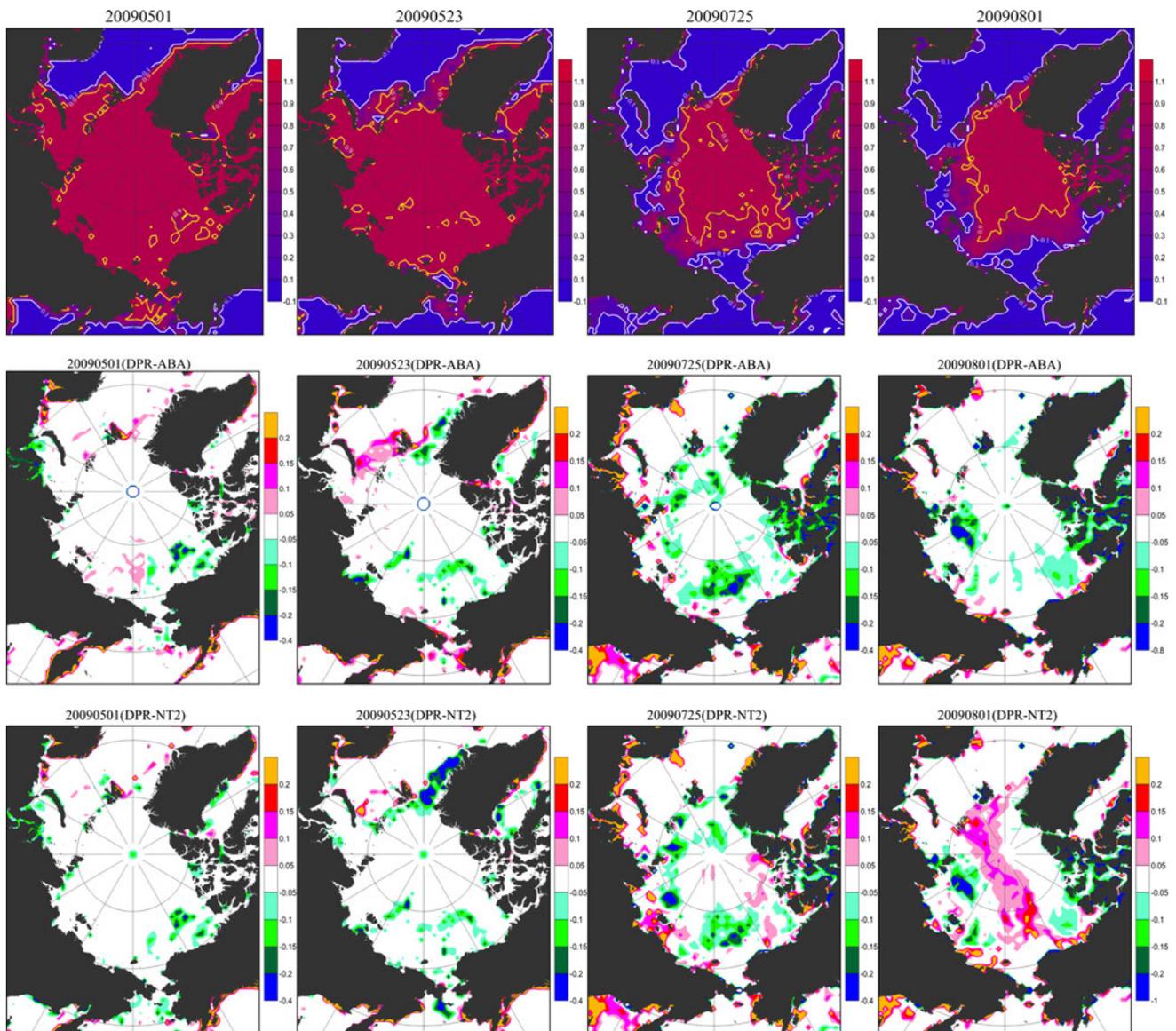
Fig. 4 Sea ice concentration retrieved by the DPR algorithm (top panels) for the days of May 1, May 23, July 25, and August 1 in 2009. The ice concentrations by the ABA and NT2 algorithms are also calculated. The differences between DPR and ABA are displayed in the middle panels, and the differences between DPR and NT2 are displayed in the bottom panels

ratio of vertically polarized sea water emissivities at 18.7 and 36.5 GHz when the ice concentration is nearly zero. When θ is smaller than β, the sea ice concentration is assigned to zero.

By now, all the parameters in Eq. (4) are determined, and sea ice concentration can be retrieved using DPR algorithm.

3 Results and validation of DPR algorithm

3.1 Results of DPR algorithm

As presented in Sect. 2, we learn that the DPR algorithm takes advantage of the physical relationship between vertically and horizontally polarized brightness temperatures at the same channel, and the microwave emissivity from sea ice surface is not necessary to retrieve sea ice concentration. With this algorithm, the sea ice concentration can be retrieved by known dual-polarized brightness temperature fields. The 12.5×12.5 km gridded AMSR-E data at 36.5 GHz are used for the DPR algorithm to obtain the sea ice concentration, some of their results in spring and summer of 2009 are shown in the top panels of Fig. 4. We also obtained the ice concentrations retrieved by the ABA and NT2 algorithms from the NSIDC. The differences between DPR and ABA are displayed in the upper-middle panels, and the differences between DPR and NT2 are presented in the lower-middle panels of Fig. 4. There is little difference between the DPR and ABA, except at the marginal ice zone. In the marginal ice zone, however, the DPR values are smaller than those of the ABA in most regions. The difference between the DPR and NT2 also exists in the marginal ice zone, but the values of the DPR during summertime are larger than those from the NT2 in the regions with high ice concentration. In the marginal ice zone, the obvious difference is caused by different algorithms, so the retrieved ice concentrations should be validated.

Note that the results generated by these algorithms show relatively high ice concentration along the coastline of
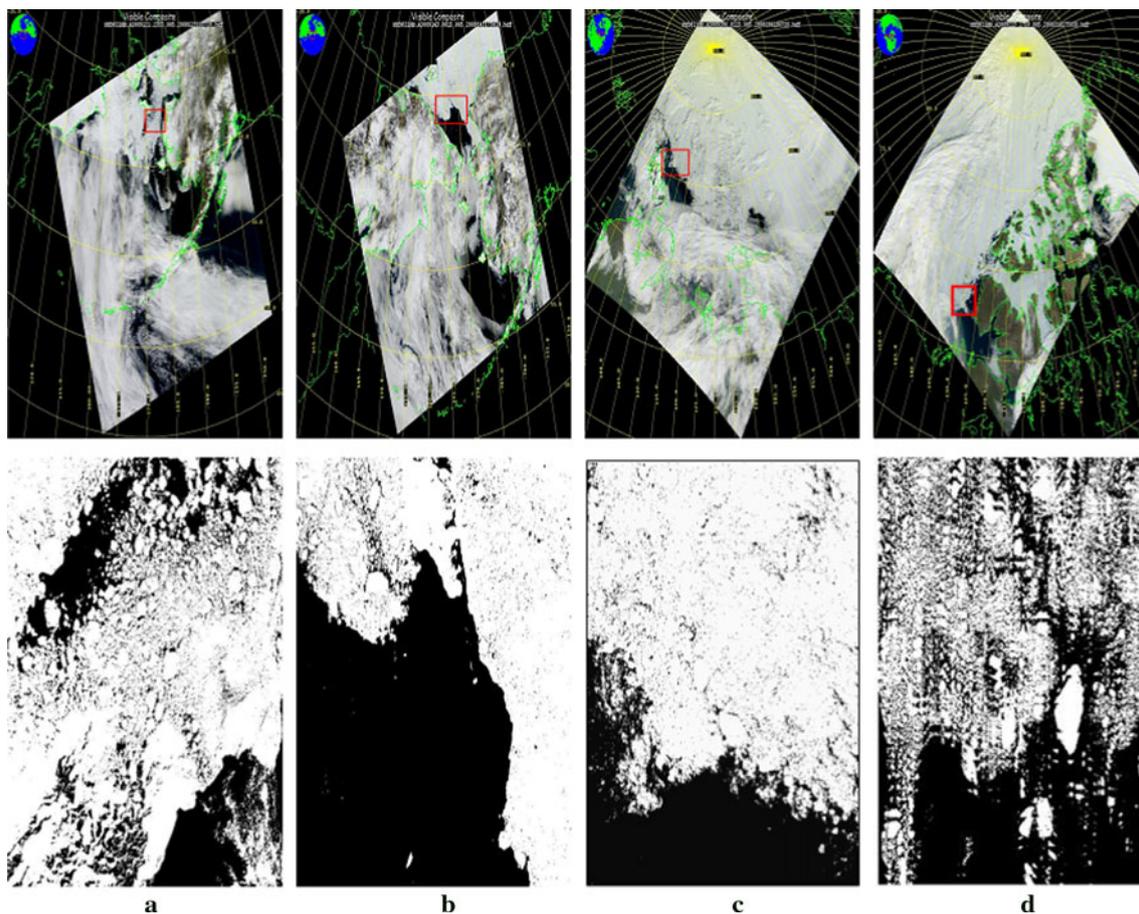
Fig. 5 MODIS images provided by NASA (http://ladsweb.nascom.nasa.gov/) and pixels of ice or water recognized by the method of Zhao and Ren (2000) in the validation regions of **a** the Bering Sea, **b** the Chukchi Sea, **c** the Barents Sea, and **d** the Beaufort Sea
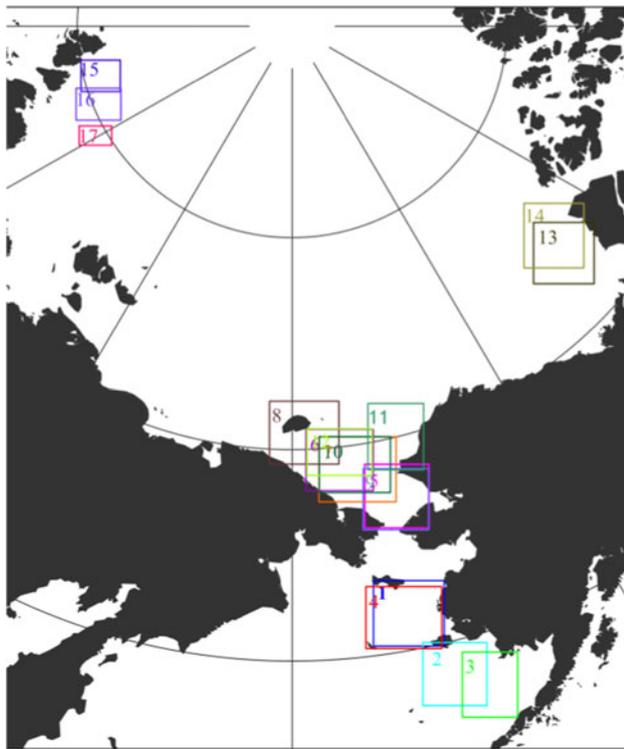
Fig. 6 Locations of validation regions. sub1–3: 23:55(UT), May 1,2009; sub4: 23:30(UT), May 21,2009; sub5–6: 23:35(UT), May 21,2009; sub 7–8: 00:15(UT), May 23,2009; sub 9–11: 23:20(UT), May 23,2009; sub 12: 23:45(UT), June 4,2009; sub 13–14: 17:50(UT), August 1; sub 15–17: 01:15(UT), July 25, 2009

Russia, which is known to be ice-free water. Comiso (1995) indicated that the brightness temperature along these coastlines represents measurements of mixtures of land and ocean, because it is difficult to discriminate land from ocean or ice covered surface. So the coastal area should be blanked out in validating the algorithms.

The MODIS has 36 channels. Channel 2 (Band 2, 841–876 nm) with 250-m resolution provides near infrared images. It is easy to discriminate water and sea ice in the MODIS data because of their highly contrasted albedo. Each MODIS pixel of 250×250 m is recognized as ice or water (Zhao and Ren 2000; Ye et al. 2011). The MODIS images and discriminated pictures are shown in Fig. 5. Figure 5a and b are for spring, and Fig. 5c and d are for summer. White and black pixels in the discriminated pictures represent ice and ocean, respectively. An AMSR-E pixel of 12.5×12.5 km is composed of 2,500 MODIS pixels. The percentage of ice pixels among the 2,500 MODIS pixels are taken as ice concentration, to be compared with the result of the AMSR-E pixels. Then, the ice concentration obtained by the MODIS is used to examine the results of the DPR, NT2, and ABA algorithms.

As mentioned above, sea ice concentrations retrieved by these three algorithms for a high concentration area are quite similar, and the main differences among these algorithms appear in the marginal ice zone. Therefore, the validation regions are chosen in the marginal ice zone, as marked by boxes in Fig. 6.

Table 1 Comparison of sea ice concentrations retrieved by the ABA, NT2, and DPR algorithms against the MODIS sea ice concentration

Regions	Gridding numbers	Mean (%)			RMS (%)			MAE (%)		
		ABA	NT2	DPR	ABA	NT2	DPR	ABA	NT2	DPR
1	493	4.32	9.56	3.20	13.56	14.86	12.35	10.01	12.28	8.62
2	415	−8.94	−2.18	−0.62	18.09	19.79	17.92	14.35	13.78	12.51
3	161	−8.45	1.48	−0.04	24.07	24.54	21.56	19.04	16.82	15.50
4	506	8.91	18.09	11.31	16.59	19.07	14.75	14.59	21.04	14.80
5	388	2.96	5.06	−2.91	*15.90*	*16.33*	*19.16*	8.36	9.11	8.69
6	432	3.92	6.02	2.23	8.43	9.34	7.14	5.83	6.55	5.17
7	484	−5.29	−2.50	−5.82	16.74	14.94	15.07	8.31	7.19	8.39
8	467	3.60	4.65	0.69	*10.24*	*10.49*	*15.41*	*5.34*	*5.55*	*6.13*
9	326	3.13	6.01	1.11	9.32	10.22	7.73	5.99	7.08	4.70
10	326	10.07	9.78	0.26	18.63	18.20	17.13	10.88	10.10	8.48
11	367	10.58	16.79	3.10	*17.99*	*21.60*	*25.86*	13.50	18.64	15.75
12	288	−11.87	−6.87	−0.69	12.41	12.11	12.91	14.09	10.13	9.62
13	291	4.98	2.26	−0.32	11.87	11.49	10.96	9.22	8.52	8.76
14	148	9.90	6.97	4.48	13.51	14.03	11.49	13.50	12.22	9.74
15	199	7.04	8.82	4.85	10.49	11.69	10.11	8.18	9.12	6.94
16	229	4.27	6.37	2.02	8.15	8.88	8.32	5.75	6.97	5.00
17	101	7.51	9.39	6.97	11.37	14.78	13.39	9.07	11.23	10.46

Gridding number is the total number of the AMSR-E in each validating region, the RMS is for the root-mean-square error, and the MAE is for the mean absolute error. The values in *italics* indicates the region where the result of the DPR algorithm is worse than that of the other algorithms
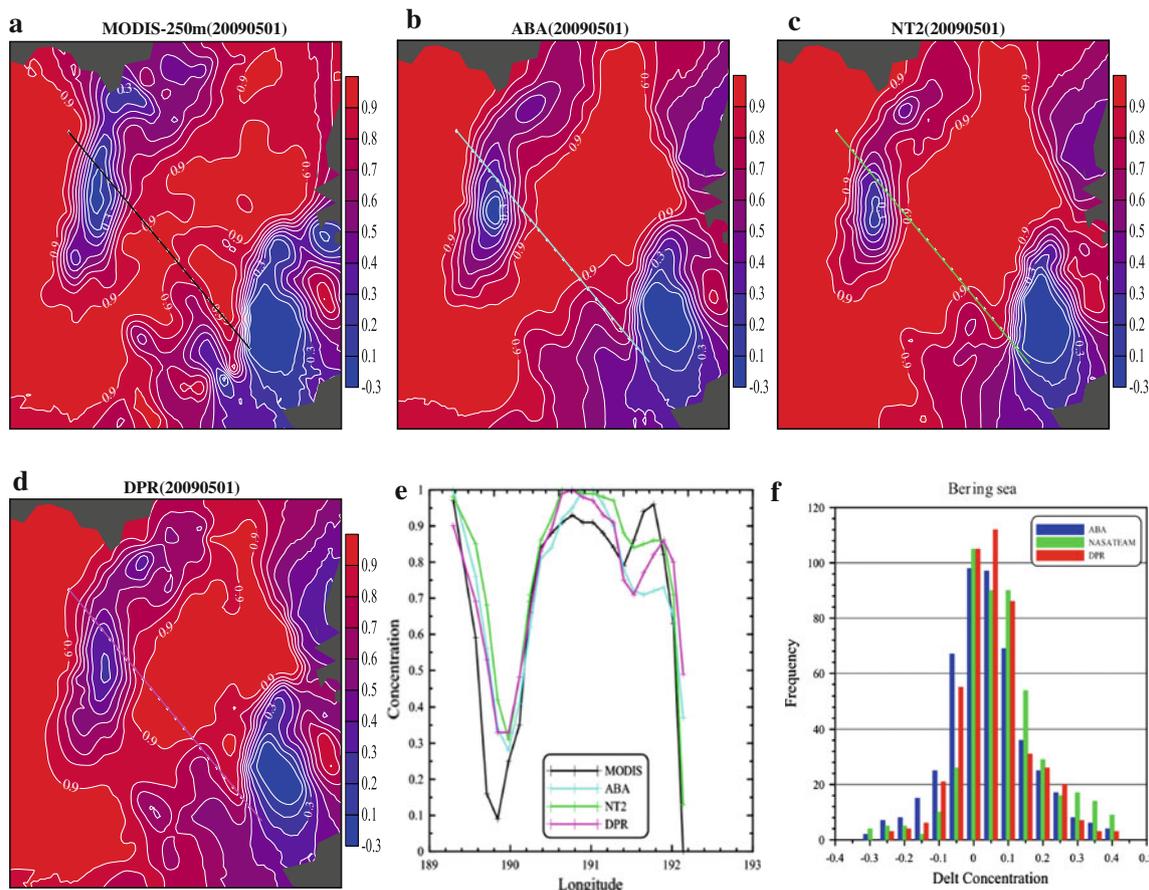
Fig. 7 Sea ice concentration from **a** the MODIS, and retrieved by **b** ABA, **c** NT2, and **d** DPR algorithms in the Bering Sea. **e** Comparison of the ice concentrations by different algorithms along the section in the figure. **f** The statistical distribution of the differences of ice concentration (Delt Concentration) from the MODIS with those by the ABA, NT2, and DPR algorithms for the whole validation region

3.2 Examination of retrieved sea ice concentration

Seventeen regions in the MIZ are chosen to compare the sea ice concentrations retrieved by the DPR, ABA, and NT2 algorithms against the MODIS image. The mean error, the root-mean-square (RMS) error, and the mean absolute error (MAE) of the ice concentrations from the MODIS image as shown in Table 1. For the mean error, the absolute value of the DPR with respect to the MODIS value is often lower than that of the ABA or NT2 in all but the 7th region where the mean error (5.82) is higher than that of the ABA (5.25) and NT2 (2.50). The RMS error of the DPR is smaller than that of the ABA or NT2 in 14 regions. Although the RMS error of DPR is larger than those of the other algorithms in the 5th, 8th, and 11th regions, the mean absolute error (MAE) of the DPR is smaller than those of the ABA and NT2, especially in the 8th region (0.69). The MAE of the DPR algorithm is better than that of the ABA or the NT2 algorithm in all but the 8th region. The comparison of the results indicates that the mean error, the RMS error, and the MAE of ice

concentration retrieved by the DPR algorithm are mostly improved, whether in summer or in spring, compared with the results by the other algorithms.

Further assessment for the accuracy of these algorithms in the validating regions is plotted in Figs. 7, 8, 9, 10. They display the validating regions of the 1st (spring), 10th (spring), 13th (summer), and 15th (summer) in the Bering Sea, Chukchi Sea, Barents Sea, and Beaufort Sea, respectively. By choosing an arbitrary section in the figures, the concentration from each algorithm along the chosen section is plotted in panel (e) of each figure. It is clear that the ice concentration retrieved by the DPR algorithm is closer to the MODIS data along these sections. Figure 7e shows that these three algorithms overestimate the ice concentration when compared with the MODIS's data. Figures 8e and 9e show that the ABA and NT2 algorithms overestimate the ice concentration, while the DPR results are very close to the MODIS's. In the Beaufort Sea, the DPR algorithm underestimates ice concentration when compared with the MODIS data for sea ice concentration exceeding 70 % (Fig. 10e). The underestimation might be
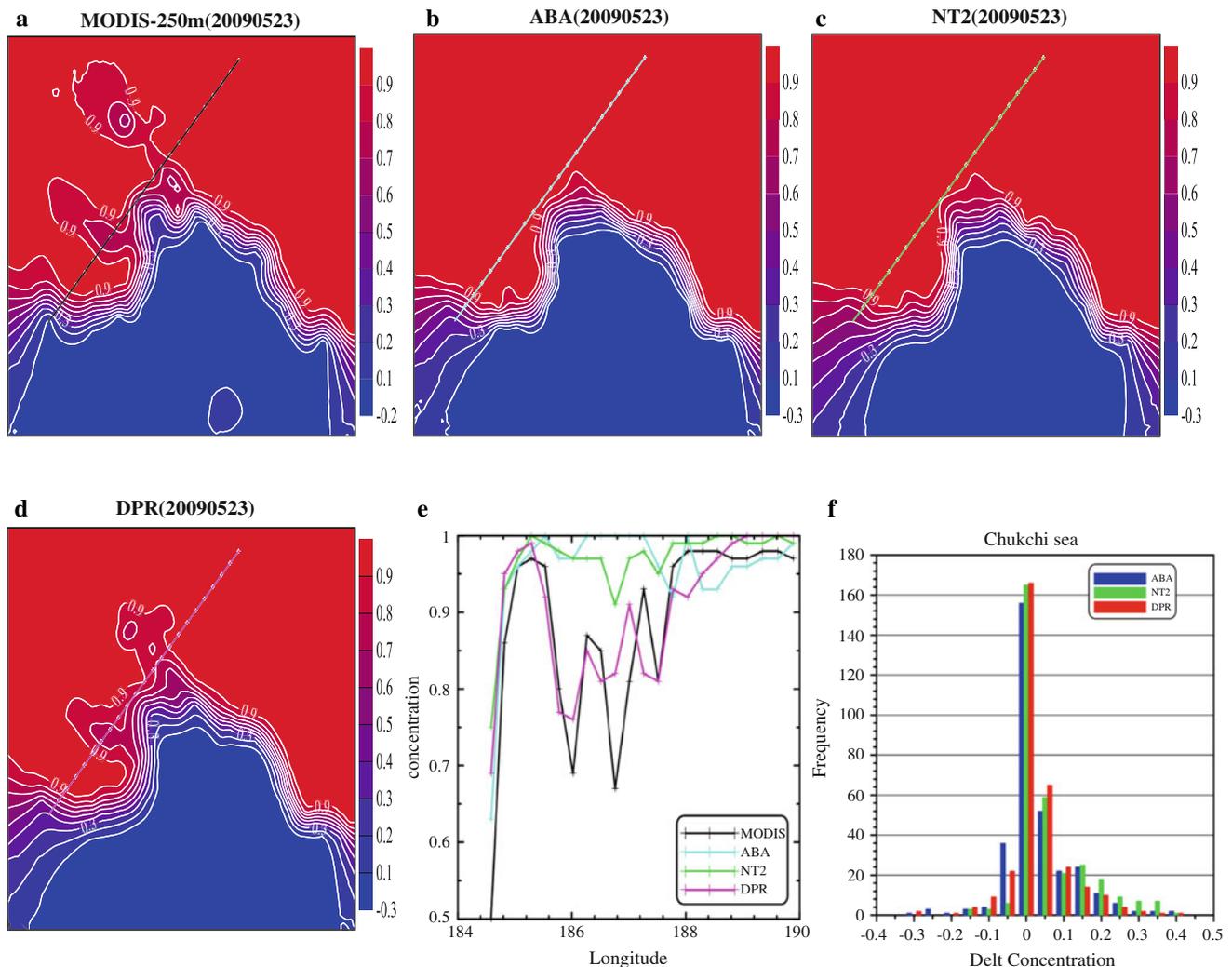
Fig. 8 Same as Fig. 7, except for the Chukchi Sea

caused by melt ponds on sea ice. Melt ponds are distinguished from ice and water by the method of Zhao and Ren (2000), and are treated as sea ice when the MODIS data are processed. Whereas large melt ponds are treated as open water by the algorithms for the AMSR-E data, which reduces the ice concentration, because the water in melt ponds has a similar microwave emissivity with that of open water (Grenfell and Lohanick 1985). Pond fractions are between 5 and 50 % in summertime (Perovich et al. 2002; Lu et al. 2010), causing the underestimation of sea ice concentration. However, when the ice under ponds totally melts, the sea ice concentration derived by the DPR algorithm would be closer to the actual ice concentration.

The statistical frequent distributions of differences in ice concentrations (Delt Concentration) of MODIS and those of the ABA, NT2, and DPR algorithms in all validation regions are displayed in panel (f) of Figs. 7, 8, 9, 10. Compared to other two algorithms, the concentrations

retrieved by DPR algorithm are most closer to those of MODIS. Therefore, sea ice concentration can be well retrieved using the DPR algorithm in the marginal ice zone.

4 The advantages of the DPR algorithm

Although DPR and ABA algorithms all used the features of dual-polarized brightness temperatures to retrieve sea ice concentration, they are fundamentally different. The ABA algorithm mainly use the geometric characteristics of sea ice emissivities, which hardly determined if there aren't low-resolution brightness temperatures (such as 6.9 GHz) (Comiso et al. 2003). However, the DPR algorithm have several advantages compared to the ABA algorithm.

One of the main advantages of the DPR algorithm is that the algorithm is derived from the serious theoretical relationship between the dual-polarized brightness temperatures
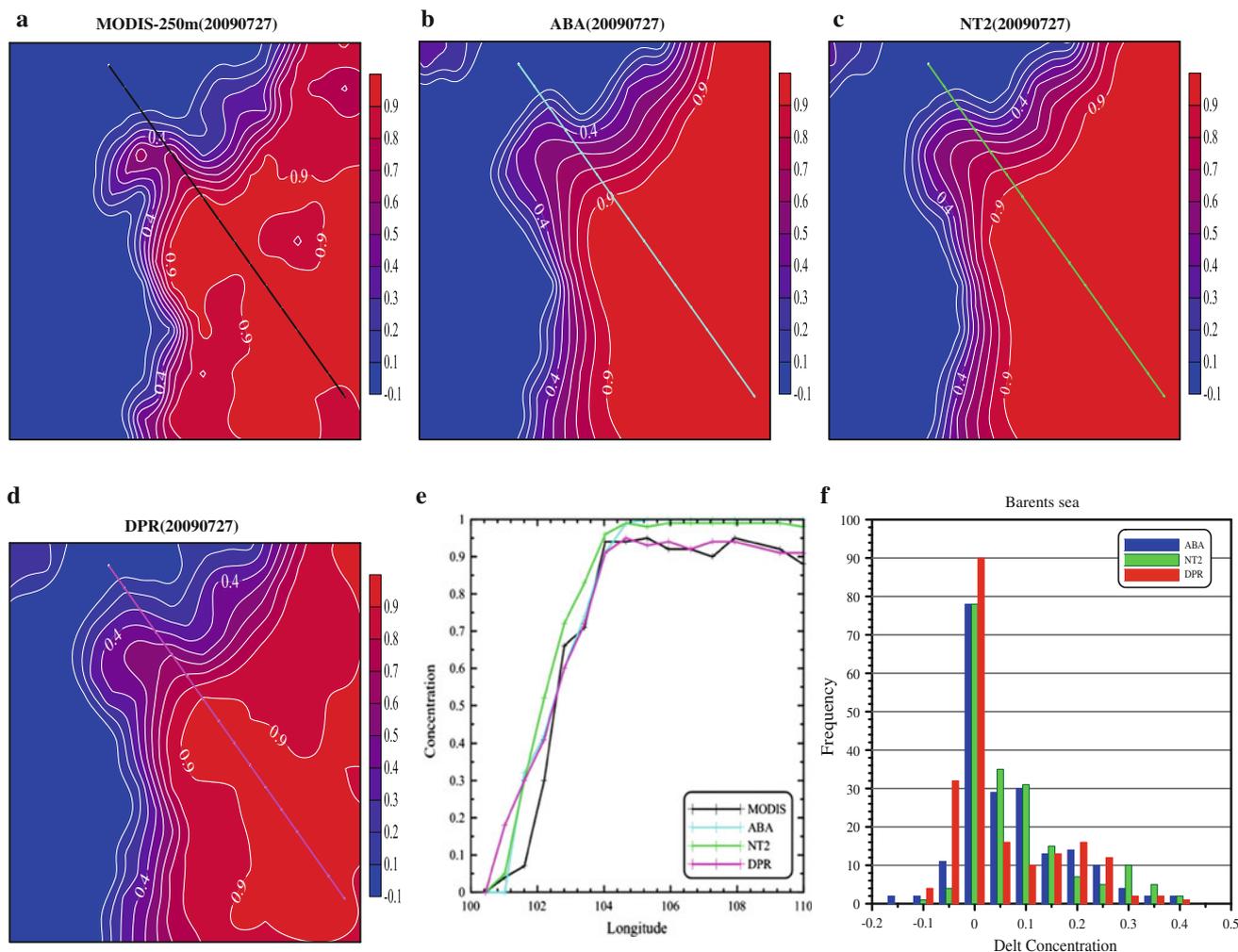
Fig. 9 Same as Fig. 7, except for the Barents Sea

and the ice concentration as expressed by Eq. (4). Therefore, the algorithm reflects the physical relevance among brightness temperature, water and ice emissivities and the ice concentration. In this algorithm, there is only one changeable parameter (α). The α is finally determined to be 0.92, as a constant value for all seasons. By this way, Eq. (4) has nothing to adjust and becomes an ideal algorithm to retrieve the ice concentration.

The α determined in this study is independent to the scatter plot in brightness temperature space (Fig. 1), but its significance is the slope of a line AD in Fig. 1. The line AD starts from the origin of the brightness temperature space and the brightness temperatures with 100 % ice concentration are clustered besides the line. The ABA algorithm also noticed the obvious linear distribution and tried to gain the line by linear regression. The regressed line depends inevitably on the scattering of the data and will bring about obvious error if the data is concentrated in a small range. Our zero-crossing line also matches the cluster of data, and

more, it depends lsess on the distribution of data as one end of the line is fixed on the origin of the space.

The zero-crossing line enables the algorithm to be valid for all seasons. There are little data for 100 % ice concentration in summer, which is not sufficient to regress a line in brightness space. The zero-crossing property of the line allows us to check if the line suits the other season's data. Although we have no sufficient evidence to verify the unchanged α for all seasons, the relevant summer brightness temperature data supports the constant α, and the retrieved ice concentration validates the algorithm with constant α.

The physical significance of α is the slope of a line in brightness temperature space, but in this paper, it is not necessary to draw the line. The α could be determined by the frequent gradient of the ratio of two polarized brightness temperatures, which in physics is the division of the pack ice with 100 % ice concentration and the ice less concentrated. It enables the Eq. (4) to form an algorithm independent to the line in brightness temperature space.
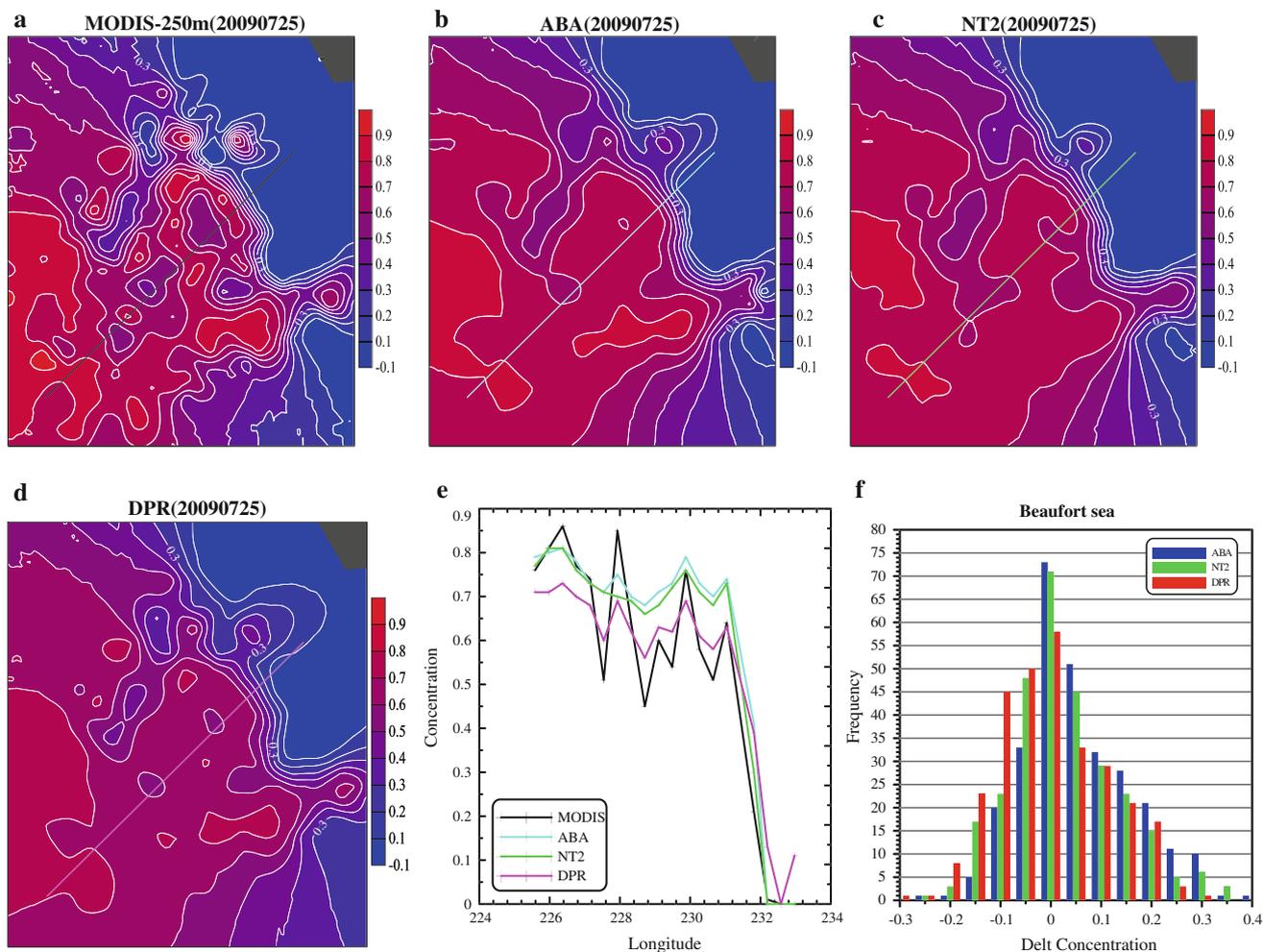
Fig. 10 Same as Fig. 7, except for the Beaufort Sea

5 Conclusions

In this study, a new algorithm for retrieving sea ice concentration from the AMSR-E data, the dual-polarized ratio (DPR) algorithm, is developed using the vertically and horizontally polarized brightness temperatures at the same channel of 36.5 GHz. The DPR algorithm avoids using the sea ice surface microwave emissivity that will bring unacceptable error to the results. The algorithm depends on the ratio of dual-polarized emissivities, α, which is determined in this study.

The dual-polarized brightness temperatures of pixels with sea ice concentration are equal to one cluster along a line (Line AD) in the brightness temperature space. The slope of this line is the ratio of dual-polarized brightness temperatures with ice concentration equal to one. It is also the ratio of the dual-polarized sea ice emissivities, α. If the ratio of the dual-polarized brightness temperatures for all ice concentration, γ, is calculated, α would be equal to a minimum γ when ice concentration equals one, which is equal to the value where the frequency number of γ changes most abruptly. Therefore, it is not necessary to regress the straight line in the brightness temperature space any more, whereas α, with a value of about 0.92, is obtained empirically by the frequency number of γ. Although α is determined by the remotely sensed brightness temperature in winter, it can be used in all other seasons as a constant. The constant value of α for all seasons cannot be derived by the brightness temperature data in summer, but the resultant ice concentration by the DPR algorithm using the winter data could be examined to verify indirectly the constant of α in other seasons.

The 12.5×12.5 km gridded dual-polarized AMSR-E brightness temperature at 36.5 GHz provided by the NSIDC is used for the DPR algorithm. The ice concentration retrieved by the DPR algorithm is compared with those of the ABA and NT2 algorithms provided by the NSIDC. The results of these three algorithms in high ice

concentration areas are quite consistent. The main differences among these algorithms take place in the marginal ice zone. Seventeen marginal ice zone regions in the Beaufort Sea, Barents Sea, Chukchi Sea, and Bering Sea are therefore chosen to retrieve ice concentration using the DPR, ABA, and NT2 algorithms. The retrieved ice concentrations are examined against the MODIS ice concentration data. The results indicate that sea ice concentration is successfully retrieved by the DPR algorithm. The mean error, RMS error, and MAE of the DPR algorithm are all more accurate compared to those of the other algorithms. It is also verified indirectly that the constant α for all seasons is valid.

In summertime, the ice concentration of the DPR algorithm is somewhat smaller than the MODIS's, which is attributed to the influence of ponds, as the water in ponds has the same microwave emissivity as open water. The results of the DPR algorithm would be closer to the actual ice concentration when the ice under a pond fully melts. It denotes that the influence of ponds on ice concentration retrieval by microwave radiation is not negligible.

The results of this study suggest that the DPR algorithm be a more accurate algorithm for retrieving sea ice concentration and therefore be used for operational purposes.

References

Aagaard K, Coachaman LK, Mack EC (1981) On the halocline of the Arctic Ocean. Deep Sea Res 28:529–545

Andersen S, Tonboe RT, Kaleschke L, Heygster G, Pedersen LT (2007) Intercomparison of passive microwave sea ice concentration retrievals over the high-concentration Arctic sea ice. J Geophys Res 112:C08004. doi:10.1029/2006JC003543

Cavalieri DJ, Gloersen P, Campbell WJ (1984) Determination of sea ice parameters with the NIMBUS 7 SMMR. J Geophys Res 89(D4):5355–5369

Cavalieri DJ, Martin S (1994) The contribution of Alaskan, Siberian, and Canadian coastal polynyas to the cold halocline layer of the Arctic Ocean. J Geophys Res 99(C9) 18: 343–18,362. doi: 10.1029/94JC01169

Comiso JC (1986) Characteristics of Arctic Winter sea ice form satellite Multispectral microwave observations. J Geophys Res 91(C1):975–994

Comiso JC (1995) SSM/I concentrations using the Bootstrap algorithm. NASA Spec Publ 1380:40

Comiso JC, Sullivan CW (1986) Satellite microwave and in Situ observations of the Weddell sea ice cover and its marginal ice zone. J Geophys Res 91(C8):9663–9681

Comiso JC, Zwally HJ (1982) Antarctic sea ice concentration inferred from Nimbus 5 ESMR and Landsat imagery. J Geophys Res 87:5836–5844

Comiso JC, Ackley SF, Gordon AL (1984) Antarctic sea ice microwave signatures and their correlation with in situ ice observations. J Geophys Res 89:662–672

Comiso JC, Cavalieri DJ, Parkinson CL, Gloersen P (1997) Passive microwave algorithms for sea ice concentration: a comparison of two techniques. Remote Sens Environ 60:357–384

Comiso JC, Member S, Cavalieri DJ, Markus T (2003) Sea ice concentration, ice temperature, and snow depth using AMSR-E data. IEEE Trans Geosci Remote Sens 41:243–252

Grenfell TC (1983) A theoretical model of the optical properties of sea ice in the visible and near infrared. J Geophys Res 88:9723–9735

Grenfell TC, Lohanick AW (1985) Temporal variations of the microwave signatures of sea ice during the late spring and early summer near Mould Bay NWT. J Geophys Res 90(C3):5063–5074

Heinrichs JF, Cavalieri DJ, Markus T (2006) Assessment of the AMSR-E sea ice concentration product at the ice edge using RADARSAT-1 and MODIS imagery. IEEE Trans Geosci Remote Sens 44(11):3070–3080

Lemke P (1987) A coupled one-dimensional sea ice-mixed layer model. J Geophys Res 92(C12):13,164–13,172

Liou KN (2002) An introduction to atmospheric radiation, chap 7, 2nd edn. Elsevier Science, Amsterdam, pp 414–419

Lu P, Li ZJ, Cheng B, Lei RB, Zhang R (2010) Sea ice surface features in Arctic summer 2008: aerial observations. Remote Sens Environ 114:693–699

Markus T, Cavalieri DJ (2000) An enhancement of the NASA Team sea ice algorithm. IEEE Trans Geosci Remote Sens 38:1387–1398

Maykut GA (1978) Energy exchange over young sea ice in the central arctic. J Geophys Res 83(C7):3646–3658

Perovich DK, Tucker WB III, Ligett KA (2002) Aerial observations of the evolution of ice surface conditions during summer. J Geophys Res. 107(C10):8048. doi:10.1029/2000JC000449

Smith DM (1996) Extraction of winter sea-ice concentration in the Greenland and Barents Seas from SSM/I data. Int J Remote Sens 17(13):2625–2646

Spreen G, Kaleschke L, Heygster G (2008) Sea ice remote sensing using AMSR-E 89 GHz channels. J Geophys Res. 113:C02S03. doi:10.1029/2005JC003384

Svendsen E, Kloster K, Farrelly B, Johannessen OM, Johannessen JA, Campbell WJ, Gloersen P, Cavalieri DJ, Matzler C (1983) Norwegian remote sensing experiment: evaluation of the nimbus 7 scanning multichannel microwave radiometer for sea ice research. J Geophys Res 88:2781–2792

Svendsen E, Matzler C, Grenfell TC (1987) A model for retrieving total sea ice concentration from spaceborne dual-polarized passive microwave instrument operating near 90 GHz. Int J Remote Sens 8(10):1479–1487

Wilheit TT (1980) Atmospheric corrections to microwave radiometer data. Boundary Layer Meteorol 18:65–77

Ye XX, Su J, Wang Y, Hao GH, Hou JQ (2011) Assessment of AMSR-E sea ice concentration in ice margin zone using MODIS data. In: Proceedings of the international conference on remote sensing environment and transportation engineering (RSETE) of IEEE

Zhao JP, Ren JP (2000) From airlines digital image extraction method of arctic sea ice form parameters. J Remote Sens 4(4):271–278

Zwally HJ, Comiso JC, Parkinson CL, Cavalieri DJ, Gloersen P (2002) Variability of Antarctic sea ice 1979–1998. J Geophys Res 107:3041. doi:10.1029/2000JC000733

Zwally HJ, Comiso JC, Parkinson CL, Campbell WJ, Carsey FD, Gloersen P (1983) Antarctic sea ice, 1973–1976: satellite passive microwave observations. Washington, DC. NASA SP-459